catalysts

MDPI

Article

Al_2O_3 Nanorod with Rich Pentacoordinate Al^{3+} Sites Stabilizing Co^{2+} for Propane Dehydrogenation

Zhiping Zhao, Zhixia Wang, Yanbing Tong, Jinru Sun, Ming Ke * and Weiyu Song *

State Key Laboratory of Heavy Oil Processing, China University of Petroleum, Beijing 102249, China;
zhao920604@163.com (Z.Z.); wzx19800318773@163.com (Z.W.); 15010095354@163.com (Y.T.);
sunjinru32@163.com (J.S.)
* Correspondence: keming@cup.edu.cn (M.K.); songwy@cup.edu.cn (W.S.)

Abstract: The search for inexpensive, environmentally friendly, and highly effective catalysts to activate C-H bonds in propane dehydrogenation (PDH) reactions is still a major challenge. Co-based catalysts have gained significant attention in recent years due to their excellent ability to activate C-H bonds and their high selectivity towards olefins, despite being a non-noble and environmentally unfriendly metal. However, further improvements are necessary for practical utilization, particularly in terms of activity and anti-carbon deposition capacity. In this study, we synthesized Al_2O_3 nanorods with abundant pentacoordinated Al^{3+} ($Al^{3+}{}_{penta}$) sites. The supported Co on the Al_2O_3 nanorod (Co/Al_2O_3-NR) exhibited higher selectivity (>96% propylene selectivity) and stability (deactivation rate 0.15 h^{-1}) compared to Co supported on an Al_2O_3 nanosheet with fewer pentacoordinated Al^{3+} sites. Various characterizations confirmed that Co(II) mainly exists as $CoAl_2O_4$ rather than Co_3O_4 in the form of Co/Al_2O_3-NR, which inhibits the reduction of Co(II) to Co^0 and accordingly improves catalyst stability.

Keywords: propane dehydrogenation; metal oxide; alumina; spinel

check for updates

Citation: Zhao, Z.; Wang, Z.; Tong, Y.; Sun, J.; Ke, M.; Song, W. Al_2O_3 Nanorod with Rich Pentacoordinate Al^{3+} Sites Stabilizing Co^{2+} for Propane Dehydrogenation. *Catalysts* **2023**, *13*, 807. https://doi.org/10.3390/catal13050807

Academic Editor: Dinesh Kumar

Received: 10 April 2023
Revised: 24 April 2023
Accepted: 25 April 2023
Published: 27 April 2023

1. Introduction

Propane dehydrogenation (PDH) reaction is a production process used in industry to produce propylene. This process has several advantages over the traditional steam cracking/catalytic cracking process, including high propylene selectivity, simple raw material and product composition, and easy separation [1–3]. The development of this process can help address the issue of increasing demand for propylene while also providing significant economic benefits.

Currently, the industry primarily utilizes Pt-Sn catalysts and Cr-based catalysts for propane dehydrogenation. The former is used in the Oleflex process, while the latter is utilized in the Catofin process [1,4]. However, due to their high cost and toxicity (in the case of CrO_X), there is ongoing research focused on developing low-cost and environmentally friendly alternatives [5,6].

Co-based catalysts are a promising candidate due to their ability to activate C-H bonds and high selectivity towards olefins [7]. It is believed that the active site of the reaction is Co(II) on the carrier, which promotes propylene desorption. Under high loading conditions, Co_3O_4 can be easily reduced to metallic Co, leading to propylene cracking [8–10]. Stabilizing Co(II) has received significant attention. Yihu Dai et al. [11] synthesized Co/Al_2O_3 using a one-step hydrothermal method. The separated Co^{2+} sites in the resulting catalyst showed high intrinsic activity (specific reaction rate > 16 mmol $g^{-1}\cdot h^{-1}$). The tetrahedral Co^{2+} isolation site was stabilized by γ-Al_2O_3 carrier, promoting propylene desorption and inhibiting coke formation and the reduction of active Co sites. Sun et al. [12] found that, at low loadings, "surface spinel" produced by tetrahedral Co^{2+} during the reaction was the active site; large particles of crystalline-Co_3O_4 were formed when loading was high, leading to increased cracking reactions and methane formation. Designing a more suitable carrier for stable Co(II) species and reducing carbon deposition is necessary.

γ-alumina (γ-Al_2O_3) is commonly used as a catalyst carrier in thermal catalysis due to its large specific surface area and good thermodynamic and chemical stability, among other properties [13,14]. Al_2O_3 contains three different states of Al^{3+}: tetrahedral Al^{3+} ($Al^{3+}{}_{tetra}$), octahedral Al^{3+} ($Al^{3+}{}_{oct}$), and pentacoordinate Al^{3+} ($Al^{3+}{}_{penta}$). The unsaturated pentacoordinate Al^{3+} is located on the surface of Al_2O_3 and can effectively anchor the active phase of the catalyst [15–18]. Liu et al. [19] synthesized stable Ru-CeO_X supported on nano-flower flake Al_2O_3 spheres rich in unsaturated pentacoordinate Al^{3+}, which were then used to catalyze the oxidation of propane. Therefore, this paper aims to stabilize Co(II) through the anchoring effect of pentacoordinate Al^{3+} with the goal of improving stability.

Here, a successful synthesis of Al_2O_3 nanorods (Al_2O_3-NR) rich in pentacoordinate Al^{3+} ions was achieved to serve as a support for Co in the PDH reaction. The pentacoordinate Al^{3+} present in the Al_2O_3-NR effectively anchors Co(II), resulting in the formation of the $CoAl_2O_4$ spinel phase that exhibits high intrinsic activity and stability. In comparison, samples without pentacoordinate Al^{3+}, such as Co(II) in Al_2O_3-NS, tend to form the Co_3O_4 phase, which can be easily reduced to Co^0, leading to rapid deactivation of the PDH reaction.

2. Results and Discussion

2.1. Catalytic Performances of Co/Al_2O_3 Catalysts

Figure 1 displays the catalytic efficiency of Co/Al_2O_3-NS and Co/Al_2O_3-NR in PDH reaction. During the initial 4 h of the reaction, propylene selectivity for both catalysts was between 90.5% to 93.5% and 96% to 97.5%, respectively. Methane, ethane, and ethylene were identified as primary by-products, with methane content being relatively high. The Co/Al_2O_3-NR catalyst exhibited an induction period of approximately one hour where conversion increased from 11% to 40.2%, followed by a slight decrease from 40.2% to 29.8% (the deactivation constant kd was found to be at a rate of 0.15 h^{-1}). In comparison with Co/Al_2O_3-NR, the conversion rate peaked at around 35% for the Co/Al_2O_3-NS catalyst before rapidly decreasing down to 17.3% (the deactivation constant kd is measured at 0.34 h^{-1}). Conversion rates for Al_2O_3-NR were slightly higher than those observed in Al_2O_3-NS, while also exhibiting better stability characteristics; indicating that carbon deposits on Al_2O_3-NR surfaces are less or have better carbon storage capacity when compared with their NS counterparts.

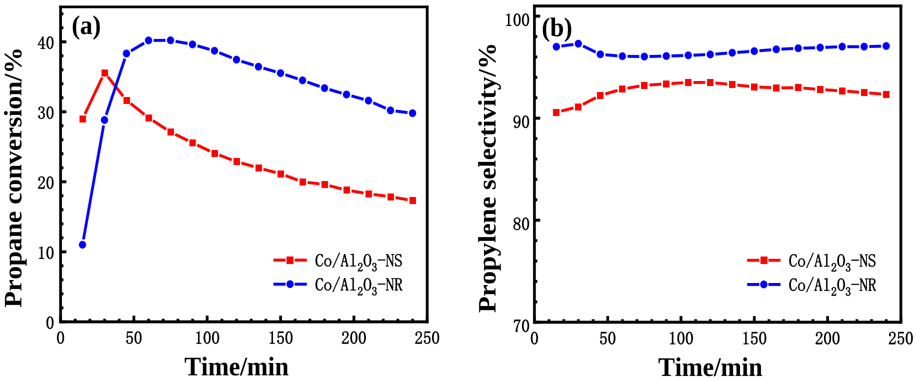

Figure 1. Propane dehydrogenation performance of Co/Al_2O_3-NS and Co/Al_2O_3-NR catalysts: (**a**) conversion; (**b**) selectivity.

A Thermogravimetric TGA analysis was conducted on the used catalyst to determine its coke content. The findings are presented in Figure 2. The temperature range of 100 °C to 300 °C is attributed to the desorption of water molecules from the surface of the catalyst, while 300 °C to 600 °C corresponds to carbon removal from the catalyst surface [20]. After reaching a temperature above 600 °C, the curve remains relatively stable. As shown in

Figure 2, Co/Al_2O_3-NS has a higher carbon deposition rate at 9.16% compared with the rate of Co/Al_2O_3-NR of only 7.54%. The result of catalytic properties and carbon deposition of Co/Al_2O_3 catalysts are shown in Table 1. This suggests that high levels of Co_3O_4 on Co/Al_2O_3-NS's surface lead to severe carbon accumulation and rapid deactivation of the catalyst. The same type of coke species is present on both catalysts, and according to the weight loss curve, the temperature range for coke deposition is between 350–450 °C. This is caused by the combustion of coke deposited on the surface of active metals and supports, which is known as hard coke and typically consists of polynuclear aromatic compounds [21].

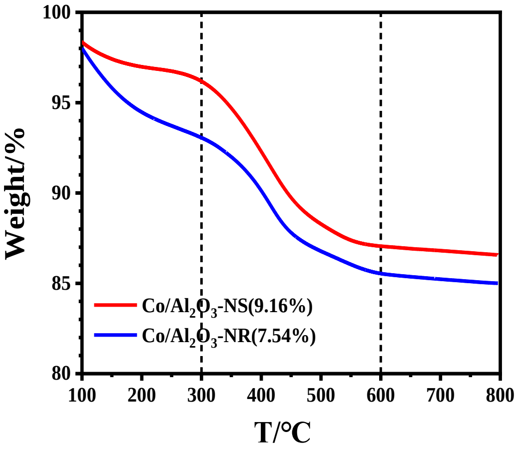

Figure 2. TGA profile of spent Co/Al_2O_3-NS and Co/Al_2O_3-NR catalysts.

Table 1. Catalytic properties and carbon deposition of Co/Al_2O_3 catalysts.

Catalyst	$Y_{propene}$, % [a]	k_d, h^{-1} [b]	Carbon Deposition, wt% [c]
Co/Al_2O_3-NS	32.4	0.34	9.16
Co/Al_2O_3-NR	38.6	0.15	7.54

[a] Ypropene represents the yield of propylene, and the maximum yield is listed in the table. [b] The deactivation rate constant, kd, was calculated based on the equation, $\ln [(1 - X_{final})/X_{final}] = kd \times t + \ln [(1 - _{xinitial})/X_{initial}]$ [22]. [c] Carbon deposition was calculated was calculated based on the TGA profile.

Figure 3 displays the activation energies of Co/Al_2O_3-NS and Co/Al_2O_3-NR during the PDH reaction. The apparent activation energy for each was measured at different reaction temperatures: 520 °C, 550 °C, 580 °C, 600 °C, and 610 °C. The results indicate that the apparent activation energy for Co/Al_2O_3-NS was found to be 147.2 kJ/mol, while that of Co/Al_2O_3-NR was found to be 202.9 kJ/mol. It is evident from these values that the dehydrogenation energy barrier for Co/Al_2O_3-NR was lower than that of Co/Al_2O_3-NS, making it more favorable towards propane dehydrogenation.

2.2. Bulk and Surface Characterization

To determine the crystal structure and composition information of the material, XRD spectra were used to analyze the catalyst. Figure 4 shows that both Al_2O_3-NS and Al_2O_3-NR detected a peak associated with γ-Al_2O_3 (PDF#29-0063), indicating that the synthesized nanorod Al_2O_3 and nanosheet Al_2O_3 are in γ-Al_2O_3 phase. Additionally, it was observed that the peak height of Al_2O_3-NS is higher than that of Al_2O_3-NR, suggesting that the crystallinity of Al_2O_3-NS is higher. After loading Co, only a peak associated with γ-Al_2O_3 can be detected, which indicates that either introduced Co species are uniformly dispersed on the surface of carrier or beyond detection range due to the small amount loaded by X-ray diffraction [23].

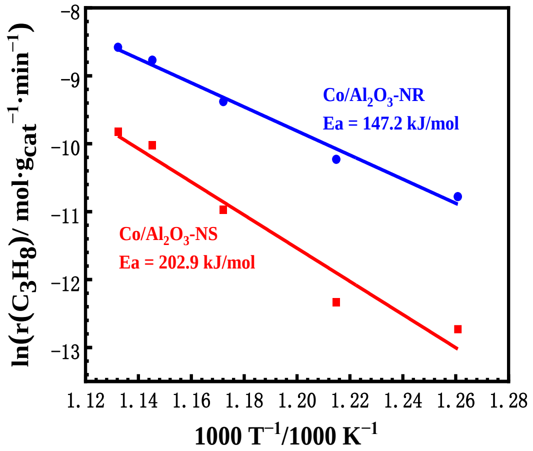

Figure 3. Arrhenius curves and apparent activation energy of Co/Al_2O_3-NS and Co/Al_2O_3-NR catalysts.

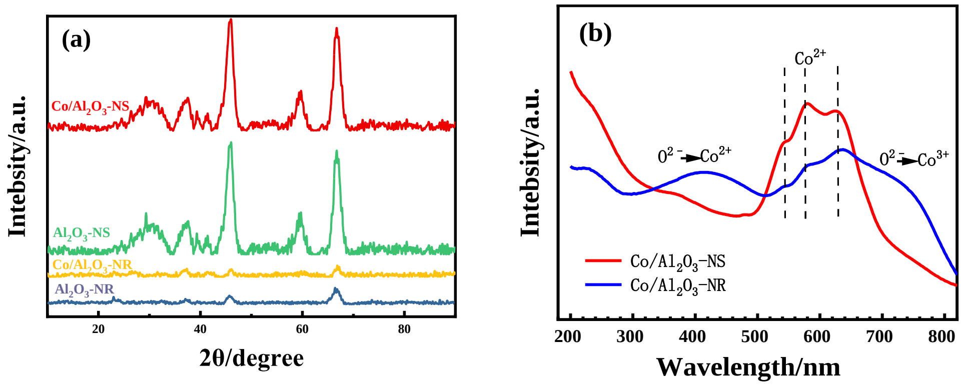

Figure 4. XRD patterns and UV-Vis spectra of Co/Al_2O_3-NS and Co/Al_2O_3-NR catalysts: (**a**) XRD; (**b**) UV-Vis.

The UV-Vis spectra (refer to Figure 4) provide details about the oxidation states and coordination geometry of cobalt species on different morphologies. In the case of Co/Al_2O_3-NR catalysts, two distinct peaks are observed at around 587 nm and 631 nm, which are attributed to the $^4A_2 \rightarrow ^4T_1$(P)d-d transition of tetrahedral (Td) Co^{2+} (the actual number of characteristic peaks is three, which may be caused by the insufficient resolution of UV-Vis spectrometers) [8,24]. No other peaks associated with other forms of Co were detected in the spectrum, indicating a normal $CoAl_2O_4$ spinel structure for the sample. Apart from these two peaks mentioned earlier, the Co/Al_2O_3-NS sample also exhibits two broad absorption bands at around 409 nm and 703 nm, respectively. These bands are related to coordination-metal charge transfer between $O^{2-} \rightarrow Co^{2+}$ and $O^{2-} \rightarrow Co^{3+}$ in Co_3O_4. Therefore, it can be concluded that while Co(II) mainly exists as $CoAl_2O_4$ in Co/Al_2O_3-NR samples, in addition to a small amount of $CoAl_2O_4$ present in them, large amounts of Co_3O_4 species along with some traces of CO(II) exist within the structure of Co/Al_2O_3-NS samples.

To analyze the element composition and chemical state of Co/Al_2O_3, X-ray photoelectron spectroscopy (XPS) was used to intercept information related to Co 2p. Figure 5 displays the XPS spectra of the Co 2p electronic energy levels in both catalysts, while Table 2 presents the binding energy and relative surface concentration of Co analyzed by XPS, along with the calculated ratio of Co^{2+}/Co^{3+}. No peak corresponding to metal Co^0 was observed on either catalyst. The four separate characteristic peaks in all Co 2p nuclear energy level spectra include two spin-orbit double peaks of Co^{2+} and Co^{3+} at positions Co 2p3/2 and 2p1/2, as well as two satellite peaks. The double peaks at position Co 2p3/2 respectively correspond to characteristic peaks of both states [11]. Peak fitting results indicate that surfaces for both types of catalysts are mainly in a state of Co^{2+}; however, the surface content is higher for Co/Al_2O_3-NR than for Co/Al_2O_3-NS. Additionally, there is a higher ratio between Co^{2+}/Co^{3+} on the former's surface compared to that on latter's surface, which suggests that it tends more towards forming $CoAl_2O_4$.

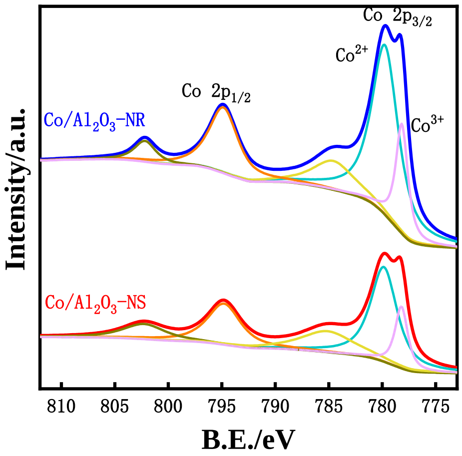

Figure 5. XPS profiles of Co/Al_2O_3-NS and Co/Al_2O_3-NR catalysts.

Table 2. XPS results of Co/Al_2O_3-NS and Co/Al_2O_3-NR catalysts.

Catalyst	Surface Concentration		Co^{2+}/Co^{3+} Molar Ratio	Binding Energy of Co^{2+} (eV)	Binding Energy of Co^{3+} (eV)
	Co, mol %	Co, wt%			
Co/Al_2O_3-NS	1.89	5.90	3.03	779.5	778.1
Co/Al_2O_3-NR	3.29	11.31	3.56	779.4	778.2

Figure 6 displays the Raman spectrum of each catalyst. Co/Al_2O_3-NS exhibits a clear Co_3O_4 structure and five Raman activity modes: A_{1g} (680 cm^{-1}), F_{2g} (616 cm^{-1}, 523 cm^{-1}, 191 cm^{-1}), E_g (480 cm^{-1}) [25,26]. No peaks related to Al_2O_3 or other Co phases are present. In comparison, Co/Al_2O_3-NR also has peaks corresponding to the Co_3O_4 structure at 680 cm^{-1} and 191 cm^{-1}. Additionally, there are peaks belonging to the $CoAl_2O_4$ structure that correspond to F_{2g} (607 cm^{-1}, 191 cm^{-1}) and E_g (480 cm^{-1}) [27]. The peak of $CoAl_2O_4$ is difficult to observe due to its weak intensity and coverage by Co_3O_4. The A_{1g} peak in the figure shows that the peak value of Co/Al_2O_3-NR is significantly smaller than that of Co/Al_2O_3- NS, indicating that less surface area on Co/Al_2O_3-NR contains Co_3O_4 and its main component is $CoAl_2O_4$.

From the above characterization, it is easy to see that in the Co/Al_2O_3-NS catalyst, Co(II) mainly exists in the form of Co_3O_4, which leads to the rapid deactivation of the catalyst. In contrast, the Co/Al_2O_3-NR catalyst has a small amount of Co_3O_4 and mostly consists of a stable spinel structure ($CoAl_2O_4$), leading to improved stability. To understand the difference between these two catalysts, ^{27}Al MAS NMR spectra of various catalysts with Al^{3+} coordination are shown in Figure 7. The proportion of Al^{3+} ions with different coordination numbers is shown in Table 3. Pure Al_2O_3 without Co showed only two different Al species in Al_2O_3-NS: octahedral Al^{3+} at about 4.13 ppm and tetrahedral Al^{3+} at about 61.8 ppm. However, in addition to these peaks, there was also a characteristic peak at about 30.7 ppm in Al_2O_3-NR attributed to pentacoordinate Al^{3+} ions (~18.5%) [28,29]. With the addition of Co, the peak corresponding to the pentacoordinate Al^{3+} ion disappeared and most of the peaks were converted into tetrahedral Al^{3+} ions. This indicates that after being impregnated, the Co particles first occupied the pentacoordinate Al^{3+} position on the surface of Al_2O_3. The disappearance of the Co-loaded NMR peak confirms that this peak is designated as Al^{3+} ions located on the surface of the Al_2O_3 support rather than lattice defect sites uniformly distributed in bulk phase [30]. The pentacoordinate Al^{3+} can anchor active centers, maintain high dispersion and thermal stability. Co(II) loaded onto a pentacoordinate Al^{3+} site on an Al_2O_3 surface is well anchored to prevent the formation of a Co_3O_4 phase, which is consistent with Raman spectrum results.

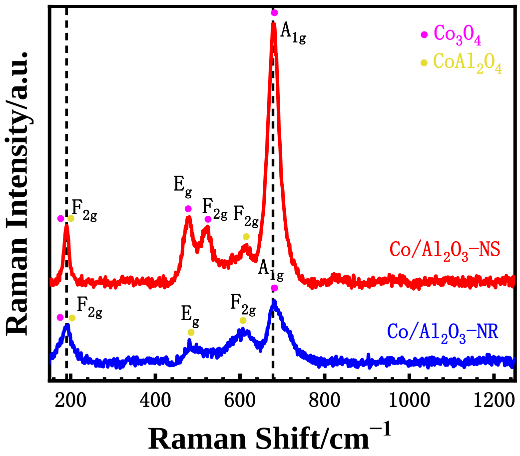

Figure 6. Raman spectra of Co/Al_2O_3-NS and Co/Al_2O_3-NR catalysts.

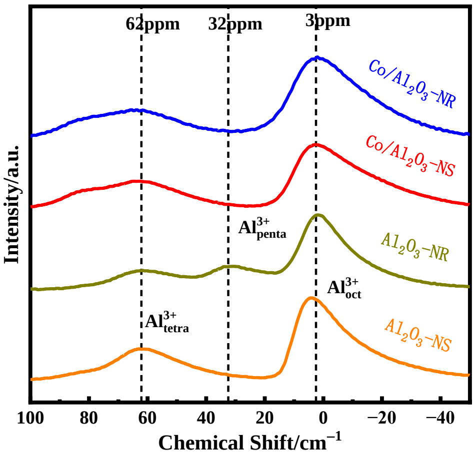

Figure 7. ^{27}Al MAS NMR spectra of Al_2O_3 and Co/Al_2O_3 catalysts.

Table 3. The proportion of different coordination Al^{3+} calculated from the peak area of ^{27}Al MAS NMR spectra.

Catalysts	Al^{3+} Coordination/%		
	Tetrahedral Al	**Pentacoordinate Al**	**Octahedral Al**
Al_2O_3-NS	31.5	-	68.4
Al_2O_3-NR	17.2	18.5	64.3
Co/Al_2O_3-NS	33.8	-	66.1
Co/Al_2O_3-NR	29.4	-	70.6

The SEM images of the Al_2O_3 support and Co-based catalyst after loading are presented in Figure 8. The Al_2O_3-NR support used in this study has a regular long rod-shaped structure, while the Al_2O_3-NS exhibits a regular sheet-like structure. Upon impregnation with 5%wt Co, there was no significant change observed on the surface of the Co/Al_2O_3-NS catalyst, and its main layered structure remained intact, indicating a high dispersion which makes its surface Co species easily reducible to Co^0, and reduces the induction period of the reaction. On the other hand, for Co/Al_2O_3-NR, the main structure still consisted of nanorods with aggregated Co oxide particles appearing at both ends of these nanorods, making them less reducible and resulting in a longer induction period compared to layered catalysts [9].

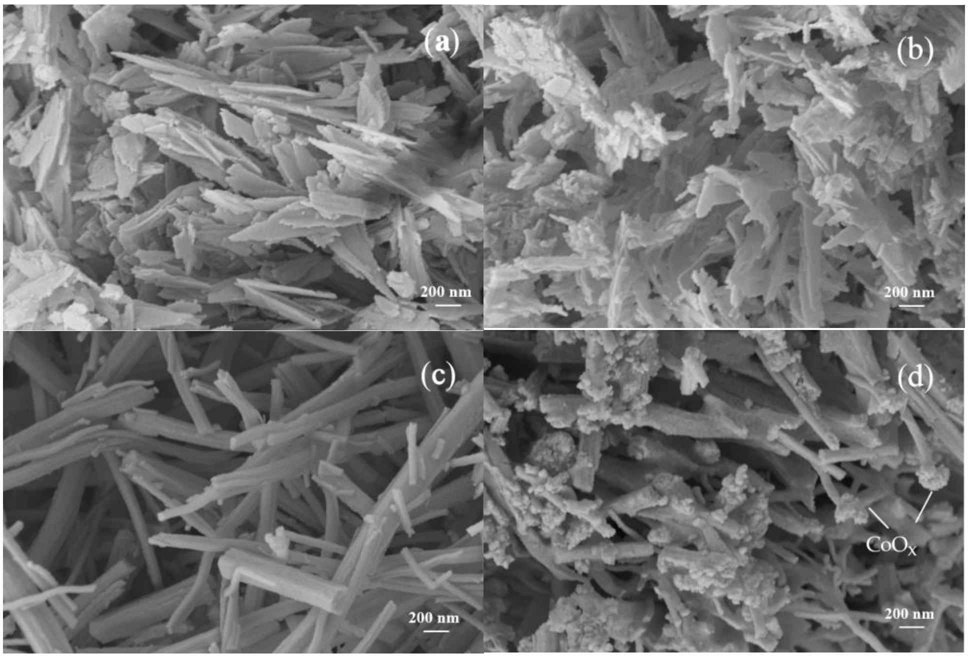

Figure 8. SEM images of catalysts: (**a**) Al_2O_3-NS; (**b**) Co/Al_2O_3-NS; (**c**) Al_2O_3-NR; (**d**) Co/Al_2O_3-NR.

2.3. Reducing Ability and Acidity of the Catalysts

H_2-TPR was used to examine how oxidized Co species in two Co/Al_2O_3 catalysts (Figure 9) behave during reduction. The Co/Al_2O_3-NS catalyst has two reduction peaks at 450 °C and 640 °C, which correspond to the reduction of Co_3O_4 to CoO and the reduction of CoO to Co^0, respectively. On the other hand, the peaks of Co/Al_2O_3-NR that correspond to the reduction of Co_3O_4 are located at lower temperatures of 420 °C and 598 °C. A comparison between these two catalysts shows that there is a stronger interaction between Co and Al_2O_3-NR under pentacoordinate Al^{3+} ions' influence, as evidenced by the shift in position for peak temperature towards higher values for Co/Al_2O_3-NS. Additionally, it is evident that there is less content of Co_3O_4 on the surface of Co/Al_2O_3-NR compared with that on Co/Al_2O_3-NS, since its peak temperature for reducing this compound is much lower; thus indicating a tendency for formation into a spinel structure mainly consisting of Co(II) and $CoAl_2O_4$.

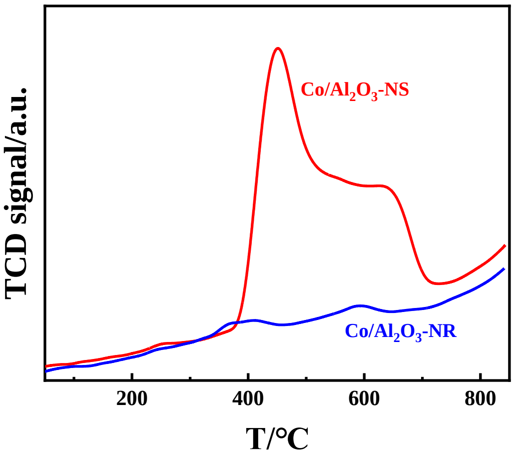

Figure 9. H_2-TPR profiles of Co/Al_2O_3-NS and Co/Al_2O_3-NR catalysts.

Figure 10 displays the results obtained from NH_3-TPD, while Table 4 presents the ratios of various acid strengths. The Al_2O_3 support exhibits weak and strong acids at approximately 160 °C and 450 °C, respectively. Upon Co loading, a medium-strength acid emerges on the surface of Co/Al_2O_3-NR and Co/Al_2O_3-NS around 215 °C. Furthermore, the strong acid present on the surface of Co/Al_2O_3-NS is significantly stronger than that found on the surface of Co/Al_2O_3-NR's, which could be another explanation for their varying carbon deposition rates. The H_2-TPR results for the two types of Al_2O_3 did not reveal any H_2 reduction peaks.

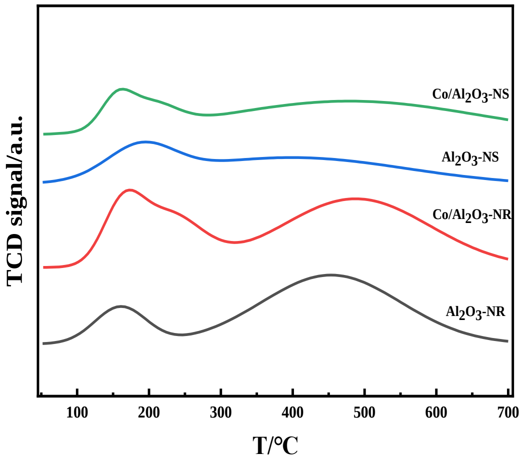

Figure 10. NH_3-TPD profiles of Co/Al_2O_3-NS and Co/Al_2O_3-NR catalysts.

Table 4. The proportion of different acid sites calculated from the peak area of NH_3-TPD.

Catalysts	Acid Sites/%		
	Strong Acid Sites	**Medium Strong Acid Sites**	**Weak Acid Sites**
Al_2O_3-NS	74.8	-	25.2
Al_2O_3-NR	83.4	-	16.6
Co/Al_2O_3-NS	79.2	12.4	8.4
Co/Al_2O_3-NR	64.5	22.4	13.1

2.4. Stability of the Catalyst

The experiment involved testing a catalyst at 580 °C for 2 h, followed by regeneration. The regenerated catalyst was then reused for six cycles, with regeneration after each cycle to study its multi-cycle catalytic activity. To regenerate the spent catalyst, a mixture of 20% O_2 and balance N_2 was used at 450 °C, followed by H_2 treatment at 580 °C. The data showed that the activity and stability were almost fully recovered after each cycle (as shown in Figure 11). Additionally, it can be observed from Figure 11 that both the regenerated and fresh catalysts exhibited similar reaction processes. Furthermore, there was little change in selectivity of the reaction conversion rate throughout the experiment.

2.5. Discussion

The Co/Al_2O_3-NR catalyst exhibits superior selectivity and stability in the propane dehydrogenation reaction compared to Co/Al_2O_3-NS. During a 4-h activity test, the inactivation rate of Co/Al_2O_3-NR was only 0.15 h^{-1}, significantly lower than that of Co/Al_2O_3-NS, indicating higher stability. To investigate this difference in stability between the two catalysts, we analyzed carbon deposition on the spent catalyst using thermogravimetry (TGA). The results showed that carbon deposition was 7.54% for Co/Al_2O_3-NR and 9.16% for Co/Al_2O_3-NS. Additionally, NH_3-TPD characterization revealed that Co/Al_2O_3-NS had a higher proportion of strong acid sites, which led to greater carbon deposition and faster deactivation compared to Co/Al_2O_3-NR. These characterizations demonstrate that surface carbon deposition is the primary cause of catalyst deactivation.

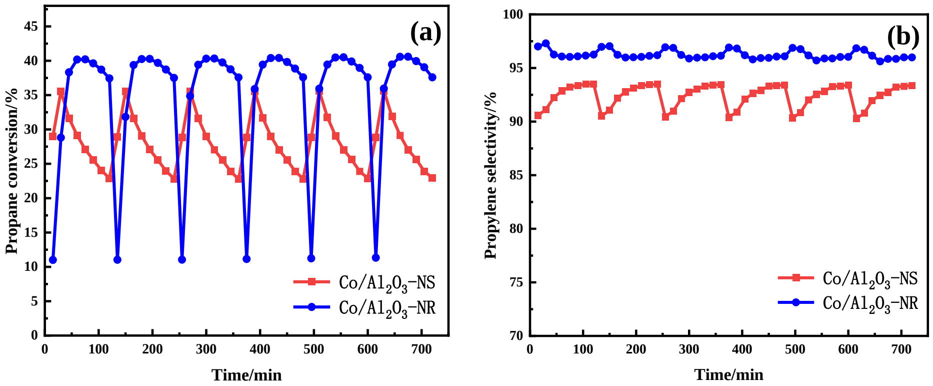

Figure 11. Regeneration property of Co/Al_2O_3-NS and Co/Al_2O_3-NR catalysts during the continuous cycles: (**a**) conversion; (**b**) selectivity.

The UV-Vis and Raman spectra indicate that Co(II) in Co/Al_2O_3 undergoes partial oxidation to form Co_3O_4. This is subsequently reduced to CoO, then to metallic Co^0 (as evidenced by H_2-TPR data). The presence of metallic Co^0 leads to propylene cracking and carbon deposition on the catalyst surface. In contrast, when interacting with Al_2O_3, Co(II) in Co/Al_2O_3-NR forms a stable spinel phase called $CoAl_2O_4$. Compared to Co_3O_4, this spinel phase is less easily reduced (the reduction peak for the spinel in H_2-TPR occurs above 700 °C). The UV-Vis spectrum shows that while there is some amount of the spinel phase present on the surface of the catalyst in both types (NS and NR), it mainly exists as Co_3O_4. This conclusion is supported by an A_{1g} peak at 680 cm^{-1} observed in the Raman spectrum. Based on H_2 consumption during H_2-TPR analysis, only a small amount of Co_3O_4 exists in the NR catalyst; most of it exists as stable structured-$CoAl_2O_4$. Therefore, two states exist for cobalt: one as unstable metallic-Co^0 from easily reducible-Co_3O_4 mostly found in NS catalysts leading to deactivation due to carbon deposition; and another state as stable structured-$CoAl_2O_4$ from less-reducible-spinels mostly found in NR catalysts which do not cause deactivation.

We have analyzed the reasons behind the formation of different Co(II) species. Our analysis suggests that the variation in surface coordination of Al_2O_3 carriers results in distinct binding energies between Co(II) and Al_2O_3, leading to two different structures: $CoAl_2O_4$ and Co_3O_4. The ^{27}Al MAS NMR spectrum indicates two states of Al^{3+} on the Al_2O_3-NS carrier—tetrahedral and octahedral—while pentacoordinate Al^{3+} is present as a defect site on the surface of the Al_2O_3-NR carrier. Upon loading, Co(II) preferentially binds to pentacoordinate Al^{3+}, resulting in spinel phase formation of $CoAl_2O_4$. This phase is more stable than the Co_3O_4 phase as an active catalyst and less susceptible to reduction by H_2 gas.

3. Methods and Materials

3.1. Catalyst Preparation

Al_2O_3 nanosheet was created using a hydrothermal method that had been previously reported. Aluminum nitrate ($Al(NO_3)_3 \cdot 9H_2O$, provided by Aladdin Biochemical Technology Co., Ltd., Shanghai, China) and urea ($CO(NH_2)_2$, provided by Guangfu Technology Development Co., Ltd., Tianjin, China) were dissolved in deionized water and stirred for 15 min until a uniform solution was formed. The concentration of $Al(NO_3)_3$ was 0.09 mol/L, with the ratio of $Al(NO_3)_3$ to $CO(NH_2)_2$ being 1:9. The solution, which had a pH of approximately 4, was then transferred to a PTFE-lined stainless steel autoclave and kept at 100 °C for 48 h. After natural cooling, the white precipitate was filtered and washed several times with deionized water and anhydrous ethanol. The powder was dried overnight at 100 °C before being calcined in air at a heating rate of 1 °C/min for two hours at a temperature of 600 °C. This resulted in the creation of Al_2O_3 nanosheet, which is referred to as Al_2O_3-NS.

The process for creating Al_2O_3 nanorods is similar to that of Al_2O_3-NS. The ratio of $Al(NO_3)_3$ to $CO(NH_2)_2$ remains at 1:9, but the concentration of $Al(NO_3)_3$ is adjusted to 0.2 mol/L. The resulting product is referred to as Al_2O_3-NR.

The method used to load Co is the impregnation method. To do this, a specific amount of cobalt nitrate ($Co(NO_3)_2 \cdot 6H_2O$, provided by Fuchen Chemical Reagent Co., Ltd., Tianjin, China) was dissolved in a small quantity of deionized water and loaded onto two different Al_2O_3 carriers using the constant volume impregnation method. The sample was then left at room temperature for 2 h, dried overnight at 70 °C, and roasted in air at 600 °C for 2 h with a heating rate of 1 °C/min. The amount of Co that was impregnated was 5 wt%. The resulting materials were named Co/Al_2O_3-NS and Co/Al_2O_3-NR, respectively.

3.2. Catalyst Characterization

The X-ray diffraction (XRD) measurement was conducted on a Rigaku C/max-2500 diffractometer (provided by Rigaku Corporation, Tokyo, Japan.) using CuKα radiation filtered through graphite (λ = 1.5406 Å), with a 2θ range of 5 to 90°.

The Raman spectrum was acquired using a RenishawinViaReex Raman spectrometer (provided by Renishaw plc, Gloucestershire, UK) with an Ar ion laser beam of 532 nm at room temperature. The data collection process involved an exposure time of 10 s and 1 accumulation. In the in situ reaction tank, the inner reaction tank is heated while the outer shell is cooled by cooling water. The gas enters into the void inside the sample tank, flows over the surface of the catalyst in a flooding manner, and then exits. Spectra are collected through the quartz glass window located on top of the sample.

Thermogravimetric analysis (TGA) is conducted using STA449F3 NETZSCH Corp (provided by NETZSCH-Gerätebau GmbH, Wittelsbacherstr, German) to examine the carbon deposition of used catalysts. The sample is first preheated in N2 (50 mL/min) at 80 °C for half an hour, and then heated in air (100 mL/min) at a speed of 10 °C/min until it reaches 800 °C.

The laboratory used self-made equipment to test H_2-TPR and NH_3-TPD. A desiccant is added before the reaction tail gas enters the TCD detector to absorb water produced by the reaction. For H_2-TPR, an appropriate amount of catalyst is treated at 350 °C under 30 mL/min N_2 for 20 min during the pretreatment stage. Then, high-purity helium is used and the sample temperature is lowered to 50 °C. During the program temperature reduction stage, a helium switch with a 10% H_2/N_2 mixture maintains a flow rate of 30 mL/min and cuts into the inlet channel of the TCD detector after stabilization of its baseline signal. The heating furnace heats up at a rate of 10 °C/min until it reaches 900 °C while detecting changes in H_2 signals online using TCD. For NH_3-TPD, dry pretreatment involves placing the sample in a reaction tube and programming the temperature from room temperature to reach up to 300 °C at a rate of 10 °C/min. He gas flow (30 mL/min) purges for about twenty minutes and then cools down to around fifty degrees Celsius before introducing mixed gas consisting of ten percent NH_3/He (30 mL/min) for thirty minutes until saturation occurs; finally, desorption attachment takes place in He atmosphere heated at ten degrees Celsius per minute until reaching seven hundred degrees Celsius while detecting outgassing through the TCD detection method.

XPS is mainly used to determine the chemical states and elemental composition of a catalyst's surface. The experiment utilizes ESCALAB220iXL (provided by Thermo Fisher Scientific Inc., Waltham, MA, USA) with monochromatic Al Kα radiation. Charge compensation is accomplished by using low-energy electrons at 10 eV, and electron binding energy is determined based on NIST's recommendation of carbon as a reference measurement at 284.8 eV.

The ^{27}Al MAS NMR was measured using a Bruker 400M high-resolution solid-state nuclear magnetic resonance (NMR) spectroscopy (provided by Bruker, Billerica, MA, USA) with a MAS spin rate of 10 Khz, a recovery time of 4 s, and a pre-scan delay of 6.5 μs.

3.3. Catalyst Tests

The PDH catalytic reaction was conducted in a fixed bed reactor under atmospheric pressure. The quartz tubular reactor had an inner diameter of 6 mm and a wall thickness of 1 mm. A catalyst loading mass of 0.2 g was used, with the catalyst being loaded in the middle of the quartz tube. Quartz cotton was filled at both ends of the catalyst, and 0.5 g of quartz sand was added to the front end. The catalyst underwent heating in nitrogen at a rate of 15 °C/min until it reached 580 °C, followed by pretreatment in H_2 atmosphere for one hour at 580 °C before conducting the PDH reaction. During this reaction, C_3H_8:N_2 = 1:19 and the total gas flow rate were maintained at 20 mL/min, respectively. An online gas chromatograph equipped with a TCD detector and flame ionization detector (FID) analyzed C_3H_8, C_3H_6, C_2H_4, C_2H_6, and CH_4 gasses; propane conversion rates as well as propylene selectivity were accordingly calculated.

Chromatographic data were analyzed using the FID area normalization method. The propane conversion rate $X(C_3H_8)$, propylene selectivity $S(C_3H_6)$, propylene yield $Y(C_3H_6)$, and propylene space-time yield $STY(C_3H_6)$ were determined using the following formula.

$$X(C_3H_8) = \frac{n(C_3H_8)_{in} - n(C_3H_8)_{out}}{n(C_3H_8)_{in}} \times 100\%$$

$$S(C_3H_6) = \frac{n(C_3H_6)_{out}}{n(C_3H_8)_{in} - n(C_3H_8)_{out}} \times 100\%$$

$$Y(C_3H_6) = S(C_3H_6) \times X(C_3H_8)$$

$$STY(C_3H_6) = \frac{n(C_3H_8)_{in} \times Y(C_3H_6) \times M(C_3H_6)}{V_m \times m_{cat}}$$

where $n(C_3H_8)$in represents the molar concentration of propane in the reactants, $n(C_3H_8)$out represents the molar concentration of propane in the product, $n(C_3H_6)$out represents the molar concentration of propylene in the product, $M(C_3H_6)$ represents the relative molecular weight of propylene, and V_m represents the molar volume of gas (22,400 mL/mol). m_{cat} represents the mass of catalyst used in the reaction and STY is measured in $kg(C_3H_6)\cdot h^{-1}\cdot kg^{-1}$.

4. Conclusions

Two different morphologies of Al_2O_3 were synthesized using the hydrothermal method and then loaded with 5 wt% Co for propane dehydrogenation reaction. The results showed that Co/Al_2O_3-NR exhibited higher selectivity and stability compared to Al_2O_3-NS. This is because Al_2O_3-NR contains a higher amount of pentacoordinate Al^{3+}, which can stabilize Co(II) particles, forming a more stable active phase $CoAl_2O_4$ spinel that is not easily reduced by H_2. On the other hand, the surface of Al_2O_3-NS does not contain pentacoordinate Al^{3+}, mainly resulting in Co_3O_4 as an active phase. However, this phase is easily reduced to metallic Co^0 leading to cracking reactions and carbon deposition. In conclusion, modifying the support morphology can further improve the activity and stability of Co-based PDH catalysts.

Author Contributions: Conceptualization, Z.Z. and W.S.; methodology, Z.Z.; validation, Z.Z., Z.W., Y.T. and J.S.; investigation, Z.Z. and Z.W.; resources, M.K.; writing—original draft preparation, Z.Z. and Z.W.; writing—review and editing, M.K.; visualization, Z.Z.; supervision, M.K. and W.S.; project administration, Z.Z. and M.K.; funding acquisition, M.K. All authors have read and agreed to the published version of the manuscript.

Funding: This research was funded by National Natural Science Foundation of China, grant number 21776303.

Data Availability Statement: The data presented in this study are available on request from the corresponding author.

Acknowledgments: This work acknowledges the financial support from the National Natural Science Foundation of China (21776303). The authors are indebted to the State Key Laboratory of Heavy Oil Processing (China University of Petroleum) for the SEM, Raman, XPS and XRD measurements.

Conflicts of Interest: The authors declare no conflict of interest.

References

1. Sattler, J.J.H.B.; Ruiz-Martinez, J.; Santillan-Jimenez, E.; Weckhuysen, B.M. Catalytic Dehydrogenation of Light Alkanes on Metals and Metal Oxides. *Chem. Rev.* **2014**, *114*, 10613–10653. [CrossRef]
2. McFarland, E. Unconventional Chemistry for Unconventional Natural Gas. *Science* **2012**, *338*, 340–342. [CrossRef] [PubMed]
3. Carrero, C.A.; Schloegl, R.; Wachs, I.E.; Schomaecker, R. Critical Literature Review of the Kinetics for the Oxidative Dehydrogenation of Propane over Well-Defined Supported Vanadium Oxide Catalysts. *ACS Catal.* **2014**, *4*, 3357–3380. [CrossRef]
4. Vora, B.V. Development of Dehydrogenation Catalysts and Processes. *Top Catal.* **2012**, *55*, 1297–1308. [CrossRef]
5. Barias, O.A.; Holmen, A.; Blekkan, E.A. Propane Dehydrogenation over Supported Pt and Pt-Sn Catalysts: Catalyst Preparation, Characterization, and Activity Measurements. *J. Catal.* **1996**, *158*, 1–12. [CrossRef]
6. Derossi, S.; Ferraris, G.; Fremiotti, S.; Garrone, E.; Ghiotti, G.; Campa, M.C.; Indovina, V. Propane Dehydrogenation on Chromia/Silica and Chromia/Alumina Catalysts. *J. Catal.* **1993**, *148*, 36–46. [CrossRef]
7. Moselage, M.; Li, J.; Ackermann, L. Cobalt-Catalyzed C-H Activation. *ACS Catal.* **2016**, *6*, 498–525. [CrossRef]
8. Hu, B.; Kim, W.-G.; Sulmonetti, T.P.; Sarazen, M.L.; Tan, S.; So, J.; Liu, Y.; Dixit, R.S.; Nair, S.; Jones, C.W. Mesoporous $CoAl_2O_4$ Spinel Catalyst for Non-Oxidative Propane Dehydrogenation. *ChemCatChem* **2017**, *9*, 3330–3337. [CrossRef]
9. Li, X.; Wang, P.; Wang, H.; Li, C. Effects of the state of Co species in Co/Al_2O_3 catalysts on the catalytic performance of propane dehydrogenation. *Appl. Surf. Sci.* **2018**, *441*, 688–693. [CrossRef]
10. Dewangan, N.; Ashok, J.; Sethia, M.; Das, S.; Pati, S.; Kus, H.; Kawi, S. Cobalt-based catalyst supported on different morphologies of alumina for non-oxidative propane dehydrogenation: Effect of metal support interaction and Lewis acidic sites. *ChemCatChem* **2019**, *11*, 4923–4934. [CrossRef]
11. Dai, Y.; Gu, J.; Tian, S.; Wu, Y.; Chen, J.; Li, F.; Du, Y.; Peng, L.; Ding, W.; Yang, Y. γ-Al_2O_3 sheet-stabilized isolate Co^{2+} for catalytic propane dehydrogenation. *J. Catal.* **2020**, *381*, 482–492. [CrossRef]
12. Sun, Y.; Wu, Y.; Shan, H.; Li, C. Studies on the Nature of Active Cobalt Species for the Production of Methane and Propylene in Catalytic Dehydrogenation of Propane. *Catal. Lett.* **2019**, *145*, 1413–1419. [CrossRef]
13. Wang, P.; Xu, Z.; Wang, T.; Yue, Y.; Bao, X.; Zhu, H. Unmodified bulk alumina as an efficient catalyst for propane dehydrogenation. *Catal. Sci. Technol.* **2020**, *10*, 3537–3541. [CrossRef]
14. Xie, Z.; Li, Z.; Tang, P.; Song, Y.; Zhao, Z.; Kong, L.; Fan, X.; Xiao, X. The effect of oxygen vacancies on the coordinatively unsaturated Al-O acid-base pairs for propane dehydrogenation. *J. Catal.* **2021**, *397*, 172–182. [CrossRef]
15. Yang, X.; Li, Q.; Lu, E.; Wang, Z.; Gong, X.; Yu, Z.; Guo, Y.; Wang, L.; Guo, Y.; Zhan, W.; et al. Taming the stability of Pd active phases through a compartmentalizing strategy toward nanostructured catalyst supports. *Nat. Commun.* **2019**, *10*, 1611. [CrossRef]
16. Duan, H.; You, R.; Xu, S.; Li, Z.; Qian, K.; Cao, T.; Huang, W.; Bao, X. Pentacoordinated Al^{3+}-Stabilized Active Pd Structures on Al_2O_3-Coated Palladium Catalysts for Methane Combustion. *Angew. Chem. Int. Ed.* **2019**, *58*, 12043–12048. [CrossRef] [PubMed]
17. Kwak, J.H.; Hu, J.; Yi, C.-W.; Kim, D.H.; Peden, C.H.F.; Allard, L.F.; Szanyi, J. Coordinatively Unsaturated Al3+ Centers as Binding Sites for Active Catalyst Phases of Platinum on γ-Al_2O_3. *Science* **2009**, *325*, 1670–1673. [CrossRef]
18. Shi, L.; Deng, G.; Li, W.; Miao, S.; Wang, Q.; Zhang, W.; Lu, A. Al_2O_3 Nanosheets Rich in Pentacoordinate Al^{3+} Ions Stabilize Pt-Sn Clusters for Propane Dehydrogenation. *Angew. Chem. Int. Ed.* **2015**, *54*, 13994–13998. [CrossRef]
19. Liu, W.; Yang, S.; Zhang, Q.; He, T.; Luo, Y.; Tao, J.; Wu, D.; Peng, H. Insights into flower-like Al_2O_3 spheres with rich unsaturated pentacoordinate Al^{3+} sites stabilizing Ru-CeOx for propane total oxidation. *Appl. Catal. B* **2021**, *292*, 120171. [CrossRef]
20. Dai, Y.; Wu, Y.; Dai, H.; Gao, X.; Tian, S.; Gu, J.; Yi, X.; Zheng, A.; Yang, Y. Effect of coking and propylene adsorption on enhanced stability for Co^{2+}-catalyzed propane dehydrogenation. *J. Catal.* **2021**, *395*, 105–116. [CrossRef]
21. Luo, S.; He, S.; Li, X.; Li, J.; Bi, W.; Sun, C. Combustion kinetics of the coke on deactivated dehydrogenation catalysts. *Fuel Process. Technol.* **2015**, *129*, 156–161. [CrossRef]
22. Jeon, N.; Seo, O.; Oh, J.; Park, J.; Chung, I.; Kim, J.; Sakata, O.; Tayal, A.; Yun, Y. Non-oxidative propane dehydrogenation over alumina-supported Co-V oxide catalysts. *Appl. Catal. A* **2021**, *614*, 118036. [CrossRef]
23. Wang, G.; Jiang, Y.; Zhang, S.; Zhu, X.; Shan, H. Insight into the Active Co Phase of Co/Al_2O_3 Catalyst for Ethane Dehydrogenation. *Catal. Lett.* **2022**, *152*, 2971–2979. [CrossRef]
24. Zayat, M.; Levy, D. Blue $CoAl_2O_4$ Particles Prepared by the Sol-Gel and Citrate-Gel Methods. *Chem. Mater.* **2000**, *12*, 2763–2769. [CrossRef]
25. Hadjiev, V.G.; Iliev, M.N.; Vergilov, I.V. The Raman spectra of Co_3O_4. *J. Phys. C* **1988**, *21*, L199–L201. [CrossRef]
26. Rivas-Murias, B.; Salgueiriño, V. Thermodynamic CoO-Co_3O_4 crossover using Raman spectroscopy in magnetic octahedron-shaped nanocrystals. *J. Raman Spectrosc.* **2017**, *48*, 837–841. [CrossRef]
27. Alvarez-Docio, C.M.; Reinosa, J.J.; Del Campo, A.; Fernandez, J.F. Investigation of thermal stability of 2D and 3D $CoAl_2O_4$ particles in core-shell nanostructures by Raman spectroscopy. *J. Alloy. Compd.* **2019**, *779*, 244–254. [CrossRef]
28. Chen, F.R.; Davis, J.G.; Fripiat, J.J. Aluminum Coordination and Lewis Acidity in Transition Aluminas. *J. Catal.* **1992**, *133*, 263–278. [CrossRef]

29. Fitzgerald, J.J.; Piedra, G.; Dec, S.F.; Seger, M.; Maciel, G.E. Dehydration Studies of a High-Surface-Area Alumina (Pseudo-boehmite) Using Solid-State 1H and 27Al NMR. *J. Am. Chem. Soc.* **1997**, *119*, 7832–7842. [CrossRef]
30. Kwak, J.H.; Hu, J.Z.; Kim, D.H.; Szanyi, J.; Peden, C.H.F. Penta-coordinated Al^{3+} ions as preferential nucleation sites for BaO on γ-Al_2O_3: An ultra-high-magnetic field 27Al MAS NMR study. *J. Catal.* **2007**, *251*, 189–194. [CrossRef]